

ARTICLE

Open Access

High sensitivity SAW hydrogen gas sensor based on thermal conductivity effect

Baile Cui¹, Lina Cheng^{1,2}, Xufeng Xue¹, Jing Jin¹, Lintaihui Huang^{1,2}, Yong Liang¹ and Wen Wang^{1,2}

Abstract

Wide-range and high-sensitivity hydrogen sensors are critically important for hydrogen safety in aerospace and advanced transportation sectors. This work demonstrates a thermal-conductivity surface acoustic wave (SAW) based sensor to achieve high sensitivity hydrogen sensing. By integrating thermal balance and acoustic wave equations, a precise mechanistic model elucidating the structure-activity relationships among gas flow rate, operating temperature, and MEMS architecture in determining sensing sensitivity is constructed. Guided by this model, the SAW hydrogen sensor with on-chip microheater integration was developed. Furthermore, a highly integrated SAW hydrogen sensing system with ultra-low baseline noise ($<30 \mu\text{V}$) was constructed for performance evaluation. Leveraging the exceptional thermal sensitivity of the SAW device and system stability, the optimized sensor achieves wide detection range (up to 100% vol), low detection limit (~ 6 ppm), rapid response and recovery time (T_{90}/T_{10} : ~ 15 s), excellent repeatability (error $< 2.4\%$) at a relatively low operating temperature (120°C). The prepared SAW sensor provides an effective solution for hydrogen leakage monitoring across unprecedented concentrations (ppm–100% vol), establishing a new paradigm for hydrogen safety applications.

Introduction

With the continuous advancement of carbon neutrality, as a secondary green energy source, hydrogen (H_2) energy holds broad application prospects in aerospace, industrial, and nuclear power sectors¹. However, H_2 is odorless, colorless, and spreads quickly. It can explode between 4–75% vol in air and needs only 0.017 mJ to ignite, making leaks highly dangerous^{2,3}. Taking leakage from an H_2 storage tank at a refueling station as an example, leakage concentrations span from ppm–100% vol in a short time⁴. Thus, hydrogen sensing with a wide range and high sensitivity is critically important for hydrogen leakage monitoring.

Typical hydrogen sensors, such as metal oxide, catalytic combustion, and electrochemical sensing technologies, feature high sensitivity and rapid response^{5,6}. However, they struggle to achieve ultra-wide-range (ppm–100% vol)

hydrogen detection and suffer from finite operational lifespans due to the adsorption saturation limitations of sensitive materials^{7,8}. Thermal conductivity effect-based hydrogen sensor is one of the most effective detection technologies for high-concentration hydrogen leakage environments, offering advantages including a broad detection range (up to 100% vol), immunity to poisoning, long service life, and fast response⁹. Common thermal conductivity-based hydrogen sensors are resistive MEMS devices, whose fundamental principle relies on hydrogen-induced perturbations to the resistance of thermosensitive elements, thereby extracting hydrogen information from resistance changes. Nevertheless, their detection limit is typically $>0.1\%$ vol, failing to meet the requirements for trace hydrogen leakage detection^{10,11}. Consequently, pursuing sensing technologies with enhanced thermosensitive effects represents a viable approach to address the low sensitivity of thermal conductivity-based hydrogen sensors.

Surface Acoustic Wave (SAW) gas sensing technology has garnered significant attention due to its high sensitivity, rapid response, and micro/nano-scale dimensions^{12–14}. A typical SAW gas sensor structure involves

Correspondence: Lina Cheng (chenglina@mail.ioa.ac.cn) or Wen Wang (wangwenwq@mail.ioa.ac.cn)

¹Institute of Acoustics, Chinese Academy of Sciences, Beijing 100190, P. R. China

²University of Chinese Academy of Sciences, Beijing 100190, P. R. China

© The Author(s) 2026



Open Access This article is licensed under a Creative Commons Attribution-NonCommercial-NoDerivatives 4.0 International License, which permits any non-commercial use, sharing, distribution and reproduction in any medium or format, as long as you give appropriate credit to the original author(s) and the source, provide a link to the Creative Commons licence, and indicate if you modified the licensed material. You do not have permission under this licence to share adapted material derived from this article or parts of it. The images or other third party material in this article are included in the article's Creative Commons licence, unless indicated otherwise in a credit line to the material. If material is not included in the article's Creative Commons licence and your intended use is not permitted by statutory regulation or exceeds the permitted use, you will need to obtain permission directly from the copyright holder. To view a copy of this licence, visit <http://creativecommons.org/licenses/by-nc-nd/4.0/>.

depositing specific gas-sensitive materials along the acoustic propagation path, of which decouples the gas information from the acoustic. Sensitive film coated SAW hydrogen sensors have achieved substantial research progress^{14,15}. Thermal conductivity-based SAW gas sensing technology modulates the operating temperature of temperature-sensitive SAW devices by exploiting thermal conductivity variations in gas mixtures. However, thermal conductivity-based SAW hydrogen sensors remain inadequately explored. V.I. Anisimkin et al. designed the thermal conductivity-based SAW gas sensor integrated with a heating film, achieving hydrogen detection in the range of 0.1–100% vol and response time of 10 min¹⁶. Tooru Nomura et al. proposed a dual-channel SAW device to solve the environmental temperature interference, and the response time was about 100 s¹⁷. In 2020, Li et al. summarized the current research progress in thermal-conductivity-based SAW gas sensing technology, highlighting that the primary challenges remain low sensitivity (>0.1% vol) and slow response speed (min level)¹⁸. Thus, research on the sensing mechanism and optimized design of high-sensitivity thermal-conductivity-based SAW gas sensors is of critical importance for enhancing the sensitivity of thermal-conductivity-based SAW hydrogen sensors.

To address these challenges, a microscale thermal conductivity-based SAW hydrogen sensor featuring a surface-integrated annular micro-heater is proposed in this study. Based on the thermal equilibrium equation and SAW propagation theory, a comprehensive thermoacoustic response model for the thermal conductivity-based SAW hydrogen sensing mechanism is established, explicitly identifying the factors influencing sensitivity. Guided by this theoretical framework, a high-performance thermal conductivity-based SAW hydrogen sensor and its integrated sensing system are fabricated. Benefiting from the high temperature sensitivity of the SAW device and the stability of the SAW hydrogen sensing system, the designed sensor achieves wide-range (up to 100% vol) hydrogen monitoring with a low detection limit (~6 ppm), which provides a novel approach for high-sensitivity thermal conductivity-based gas sensing technology.

Design and simulation

Structure and sensing mechanism

The fundamental structure of the designed thermal conductivity-based SAW hydrogen sensor is shown in Fig. 1a. An annular micro-heater is symmetrically positioned around the periphery of the SAW device to elevate its operating temperature via joule heat. The symmetrical structure facilitates uniform temperature distribution on the SAW device surface through symmetrical thermal conduction, thereby ensuring SAW propagation stability. To enhance sensing sensitivity, lithium niobate

piezoelectric crystal is selected as the substrate for theoretical analysis. The operational process involves the micro-heater raising the SAW device's operating temperature, which in turn is perturbed by changes in the thermal conductivity of the gas mixture. This enables temperature-induced perturbations to SAW propagation characteristics based on the thermoacoustic transduction mechanism.

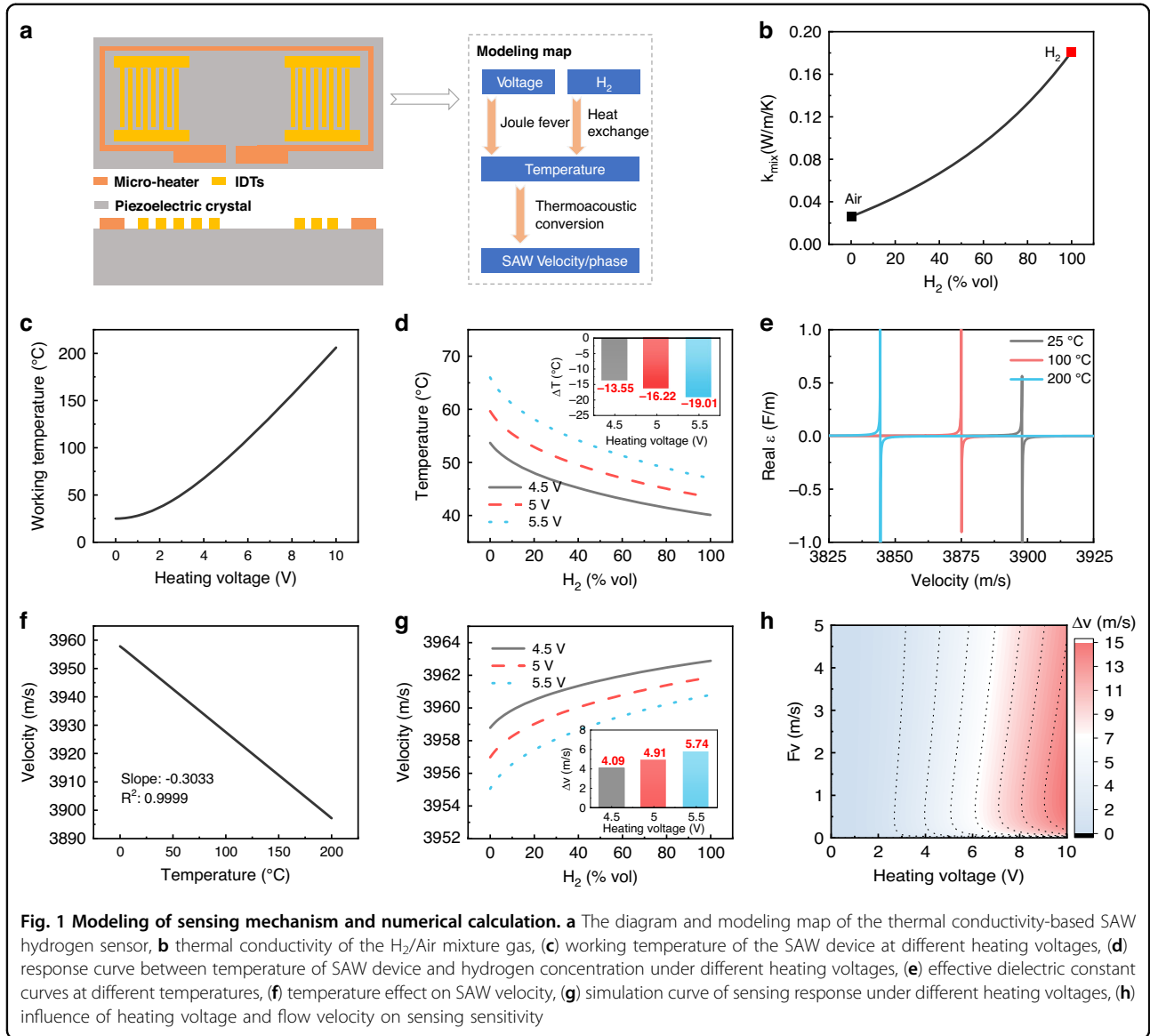
To establish a simulation model for the thermal conductivity-based SAW hydrogen sensor, the following assumptions are made: (1) The perturbation of the input signal from the interdigital transducers (IDTs) on the device surface temperature and the thermal loss of the IDTs themselves are neglected. (2) Heat loss due to thermal radiation is disregarded. Based on the law of conservation of energy, the internal energy Q of the heated SAW device can be expressed as:

$$Q = Q_{cq} + Q_{cp} + Q_v + P_{in} + Q_0 \quad (1)$$

Here, Q_{cq} , Q_{cp} , Q_v and Q_0 represent the heat dissipation of the piezoelectric crystal, heat loss through external thermal contacts, convective heat loss to the surrounding environment, and the internal energy of the device at ambient temperature, respectively. The heating power of the micro-heater is given by $P_{in} = \frac{V^2}{R}$, where V is the heating voltage of the micro-heater and R is the resistance of the micro-heater. Considering the relationship between resistance R and temperature change ΔT , $R = R_0(1 + \alpha\Delta T)$, where α is the temperature coefficient of resistance and R_0 is the initial resistance¹⁹. By incorporating Fourier's law and Newton's law of cooling into Eq. (1), the transient heat transfer equation for the SAW device can be derived:

$$M_e C_e \frac{d(T - T_a)}{dt} = - \left(\frac{k_q A_h}{t_q} + \frac{k_e A_e}{t_e} + \sum_{i=1}^6 h_i A_i \right) (T - T_a) + \frac{V^2}{R_0(1 + \alpha\Delta T)} \quad (2)$$

In the above equation, M_e and C_e represent the equivalent heated mass and equivalent specific heat capacity, respectively; k_q denotes the thermal conductivity of the piezoelectric crystal; A_h is the contact area between the micro-heater and the piezoelectric crystal; t_q is the thickness of the piezoelectric crystal; k_e is the equivalent thermal conductivity between the piezoelectric crystal and other thermal contacts; A_e is the contact area at the thermal interface; t_e is the heat transfer distance of the thermal contact; T is the time-dependent temperature; T_a is the ambient temperature; h_i represents the convective heat transfer coefficients for the six surfaces of the SAW device; and A_i is the area of each of the six surfaces $i=1,2,\dots,6$. Under steady-state conditions, $\frac{d(T - T_a)}{dt} = 0$. Thus, the expression for the temperature change ΔT of



the SAW device is:

$$\Delta T = \frac{-G_{eq}R_0 + \sqrt{(G_{eq}R_0)^2 + 4\alpha G_{eq}R_0 V^2}}{2\alpha G_{eq}R_0} \quad (3)$$

Where $\Delta T = T - T_a$, equivalent thermal conductivity $G_{eq} = \frac{k_q A_h}{t_q} + \frac{k_e A_e}{t_e} + \sum_{i=1}^6 h_i A_i$, the convective heat transfer coefficients are as follows:

$$h = \frac{\overline{Nu} \times k_{mix}}{L} \quad (4)$$

where \overline{Nu} is the average Nusselt number, k_{mix} is the thermal conductivity of the gas mixture, and L is the

characteristic length. The theoretically calculated thermal conductivity of hydrogen/air mixtures is shown in Fig. 1b (simulation parameters in Table S1 of supplementary information and calculation formula in Note S1 of supplementary information). Evidently, increasing hydrogen concentration enhances the thermal conductivity of the mixture. These results align closely with calculations by Masaya Watanabe et al¹¹, validating the effectiveness of the computational model. Furthermore, the operating temperature of the SAW device increases with rising heating voltage due to joule heating (Fig. 1c). To analyze the influence of hydrogen on the operating temperature, computations were performed for 0–100% vol H₂ at heating voltages of 4.5 V, 5 V, and 5.5 V (Fig. 1d). While higher initial operating temperatures were achieved with increased voltage, the significantly greater thermal

conductivity of hydrogen compared to air caused a sharp decrease in device temperature ($>13^{\circ}\text{C}$) as hydrogen concentration rose. This temperature variation intensified with higher initial operating temperatures, indicating that elevated operating temperatures enhance sensing sensitivity.

To further examine the perturbation mechanism of temperature on SAW propagation, this study employs the acoustic wave equation and the effective permittivity method to rapidly calculate SAW velocity at different temperatures. The effective permittivity, as defined by Milsom et al., is given by²⁰:

$$\varepsilon_s(s) = \frac{\tilde{\sigma}(s)}{\omega|s|\tilde{\Phi}(s, x_3)|_{x_3=0}} \quad (5)$$

Here, $\varepsilon_s(s)$ represents the effective permittivity, $\tilde{\sigma}(s)$ denotes the surface conductivity, ω is the angular frequency, $|s|$ is the slowness, and $\tilde{\Phi}(s, x_3)$ is the surface potential. By incorporating temperature as a factor in the wave equation, the effective permittivity curve at different temperatures is solved, thereby revealing the temperature sensitivity of the SAW device. The simulation parameters of LN are the experimental data of Smith²¹. The calculated effective permittivity curves are shown in Fig. 1e. As the device temperature increases, the effective permittivity curve progressively shifts toward lower frequencies, indicating an inverse correlation between SAW velocity and temperature. This is confirmed by the SAW velocity curves at different temperatures in Fig. 1f. The SAW velocity decreases by 0.3033 m/s per $^{\circ}\text{C}$. Furthermore, the SAW device based on a 128 $^{\circ}\text{YX}$ -LN substrate exhibits excellent linearity ($R^2: >99.99\%$), implying that temperature can be linearly decoupled from the SAW velocity. Consequently, hydrogen concentration information can also be decoupled. As shown in Fig. 1g, higher heating voltages lead to an increase in SAW velocity with rising hydrogen concentration. Increasing the heating voltage (i.e., elevating the sensor temperature) enhances the sensing response sensitivity. Benefiting from the linear and negative velocity-temperature coefficient of the SAW device (Fig.1f), the variation trend of SAW velocity in Fig. 1g exhibits a strong inverse correlation with the trend of temperature variation. Additionally, to clarify the influence of external perturbation factors on sensing sensitivity, the theoretically calculated response sensitivity S is defined as:

$$S = \frac{\Delta v}{c} \quad (6)$$

where Δv represents the change in SAW velocity and c is the hydrogen concentration. Taking $c = 1$ estimates the full-range sensitivity of the thermal conductivity-based

SAW hydrogen sensor. Figure 1h illustrates the sensitivity map under varying hydrogen flow rates and device heating voltages. The results reveal that the sensing response sensitivity increases with higher heating voltages. However, a distinct nonlinear relationship exists between flow velocity (Fv) and sensing sensitivity. Flow rates enhance the heat exchange process between the device and hydrogen, while higher flow rates increase the Reynolds number, reducing the operating temperature and consequently diminishing sensitivity. Clearly, achieving high sensitivity in SAW hydrogen sensors requires balancing the heating voltage and flow velocity. Additionally, the surface heat transfer coefficient is closely related to device dimensions. Figure S1 of the supplementary information demonstrates that reducing device size improves sensitivity, though this effect is less pronounced than that of flow velocity. Given the relationship between SAW velocity and phase shift:

$$\Delta\varphi = -\frac{\Delta v}{v_0}\varphi_0 = -2\pi f_0 \frac{\Delta v}{v_0^2} L_s \quad (7)$$

where f_0 is the operating frequency of the SAW device, and L_s is the SAW propagation path length. As evident from Eq. (7), gas sensing utilizing SAW phase shift allows sensitivity manipulation by controlling the acoustic propagation path. Specifically, under identical SAW velocity changes, increasing the acoustic propagation path length enhances the sensing response sensitivity. Thus, thermal conductivity-based SAW hydrogen sensing technology, which employs phase as the sensing metric, possesses theoretical potential for higher sensitivity.

Design and preparation of the SAW sensing device

A delay-line SAW device was used for hydrogen sensing, and 200 MHz was chosen as the working frequency of the SAW chip after considering the gas sensing sensitivity and sensor cost. Aluminum input and output interdigital transducers (IDTs) were deposited on the surface of a 128 $^{\circ}\text{YX}$ -LN piezoelectric crystal using standard photolithography. The IDTs adopted an apodized unidirectional single-phase transducer structure to achieve unidirectional acoustic wave propagation, thereby reducing SAW propagation loss and enhancing sensing accuracy²². The micro-heater was fabricated using the same process as the IDTs and positioned at the periphery of the SAW propagation region to avoid disturbing SAW propagation. Detailed structural parameters of the device are listed in Table 1. Additionally, two SAW sensors with distinct SAW propagation path lengths were designed to comparatively analyze the impact of phase modulation on the sensitivity of the thermal conductivity-based SAW hydrogen sensor.

Fig. 2a displays the fabricated SAW sensing chip wafer based on the aforementioned device parameters, exhibiting a smooth and intact surface. Figure 2b presents a single thermal conductivity-based SAW device with

dimensions of 6 mm × 3 mm. The fabricated single-phase unidirectional IDT structure closely matches the theoretical design²³. Furthermore, dummy finger structures are uniformly distributed in the input IDTs to enhance the stability within the bandwidth of the SAW device²⁴. Electrical characterization of the SAW device using an Agilent E5061B network analyzer reveals low insertion loss (~ -10 dB, Figure S2 of the supplementary information) and linear phase characteristics (Fig. 2c) at the operating frequency of 200 MHz, ensuring signal stability during sensing operations. By applying DC voltage to the micro-heater and employing infrared thermography, the relationships between heating voltage vs. power consumption and heating voltage vs. operating temperature were obtained (Fig. 2d). Experimental results align closely with theoretical simulations (Fig. 1c). Figure 2e illustrates the relationship between the 200 MHz phase response and operating temperature (real-time response curve in Figure S3a of the supplementary information). The SAW device based on the 128°YX-LN substrate demonstrates linear temperature sensitivity, enabling accurate temperature extraction from phase variations. Furthermore, experimental results show excellent agreement with calculations using the effective permittivity method, validating the computational model. Moreover, a linear fitting of the relationship between temperature and phase (Fig. S3b of the supplementary information) exhibits that a temperature change of 1°C induces a phase

Table 1 Detailed structure parameters of the SAW device

Parameters	Values
Substrate	LiNbO ₃
Orientation	128°Y
IDTs materials	Aluminum
Wavelength (λ)	19.45 μm
Exciting finger width	0.125λ
Reflecting finger width	0.25λ
Thickness of IDTs	120 nm
Length of wave propagation path	200λ/100λ
Number of exciting IDTs	15
Number of false fingers	20
Number of output IDTs	15
Aperture of IDTs	80
Microheater materials	Aluminum
Thickness of microheater	120 nm
Length of microheater	270λ/170λ
Width of microheater	130λ

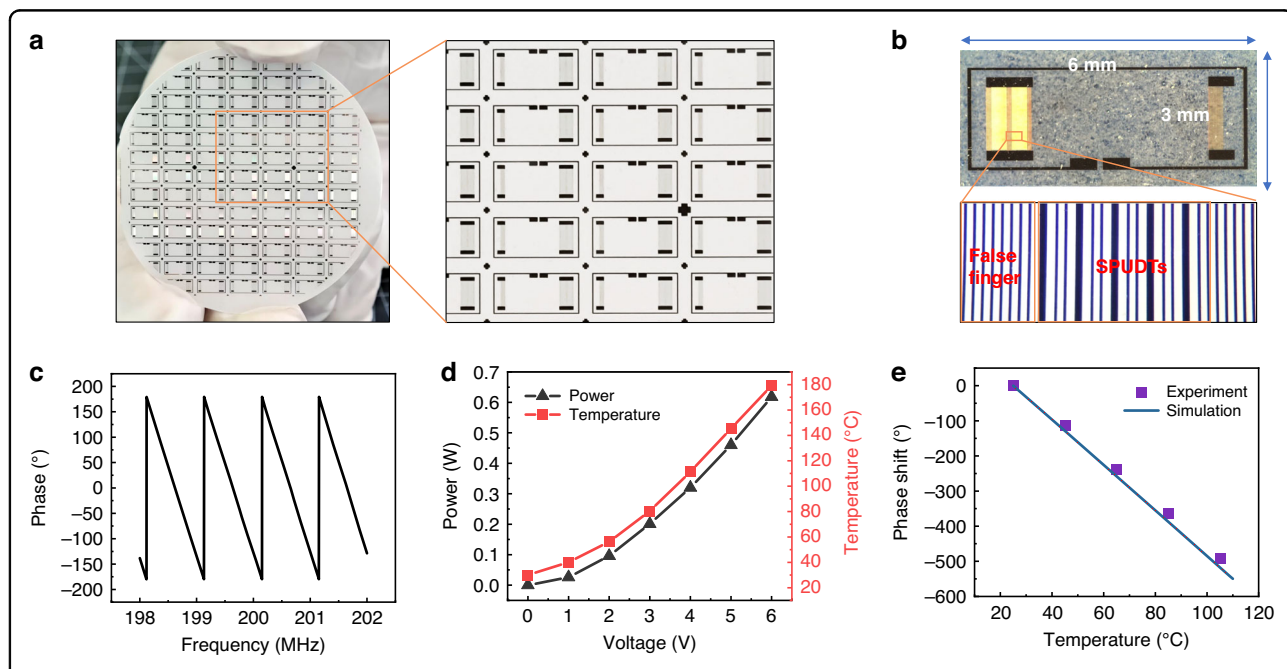
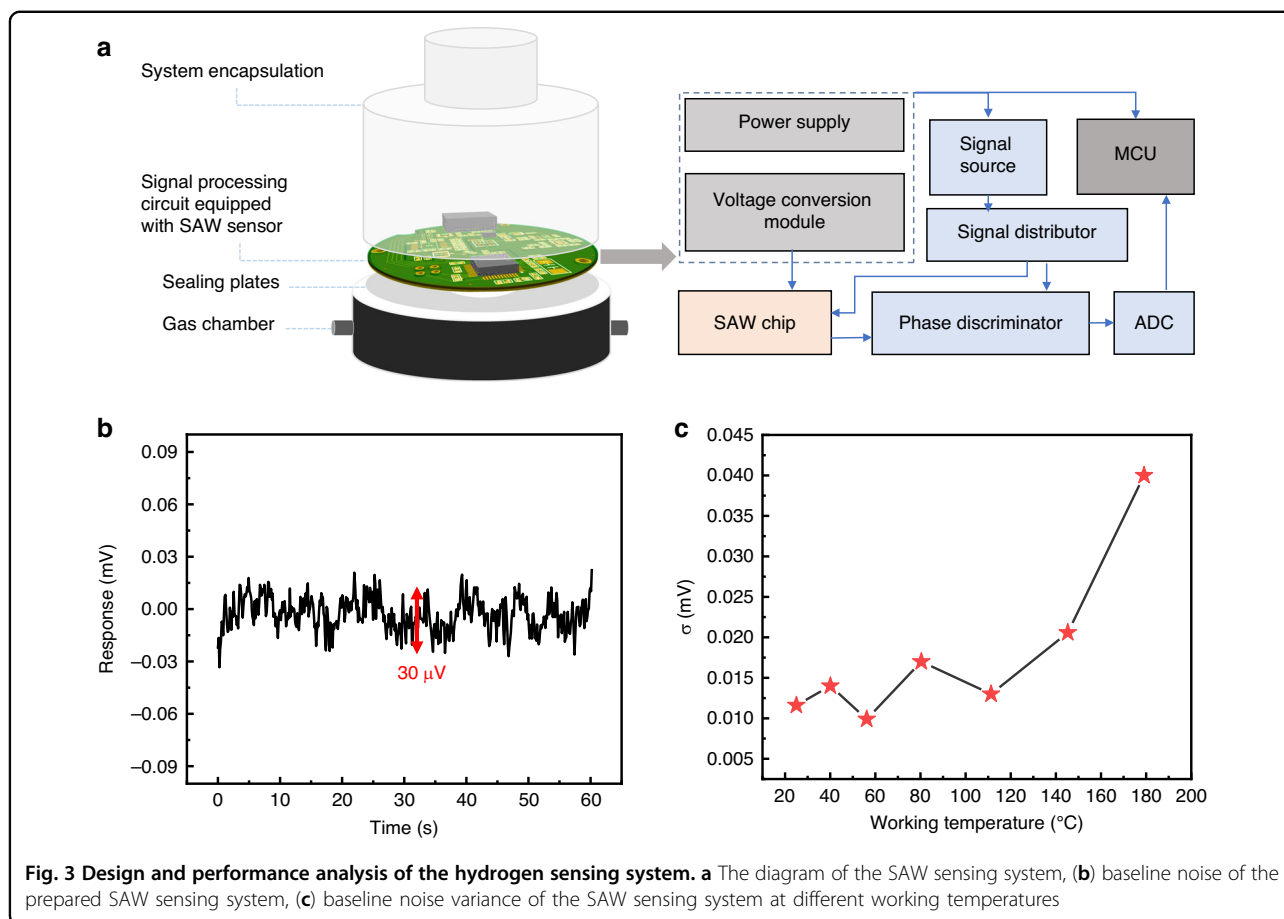


Fig. 2 Fabrication of SAW sensor devices and their performances. **a** The wafer of the thermal conductivity-based SAW sensor, **(b)** the structure of the SAW chip and IDTs, **(c)** the phase response of the SAW device, **(d)** the working temperature and power consumption of the SAW device under different heating voltages, **(e)** phase shift comparison between simulation and experiment at different working temperatures



shift of -6° , which is beneficial to realize high-sensitivity hydrogen sensing.

Results and discussion

SAW sensing system

To enable acoustic excitation and signal acquisition for the SAW device, a SAW gas sensing system architecture was shown in Fig. 3a. It comprises a sealed gas chamber, sealing plate, SAW device, SAW signal processing board, and mechanical packaging. The mechanical encapsulation of the sensing system employs a robust stainless-steel structure to enhance the reliability and safety of the sensor in high-concentration hydrogen environments. Furthermore, a hermetically sealed plate effectively isolates the hydrogen atmosphere from direct contact with the signal processing circuitry, thereby preventing potential adverse effects of high-concentration hydrogen on the electronic components within the sensing system. This design ensures operational integrity while complying with essential safety requirements for hydrogen applications. The SAW device is bonded to a beam-mounted base using rubber adhesive, with electrical connections established through wire bonding between the SAW device signals and the base (Fig. S4a of the supplementary

information). Connections between the device and printed circuit board (PCB) are implemented via soldering. To ensure stable and reliable hydrogen sensing performance testing, a metal gas chamber and metal sealing plate isolate the SAW device from the signal processing circuitry. This design maintains the SAW device in a stable gas environment while preventing high-concentration hydrogen from contacting the signal processing board, thereby enhancing system reliability and stability. The SAW signal circuit architecture includes power supply and voltage conversion module. RF signal generator, signal processor, signal splitter, sensing module, phase detector, and ADC chip. Its fundamental operating principle aligns with our previously reported work²⁵. Phase information from the SAW device is converted to a linear voltage output ($1^\circ = 10 \text{ mV}$) using the AD8302 phase detector. The fabricated PCB (Fig. S4b of the supplementary information) has a diameter $<5 \text{ cm}$. Benefiting from the excellent SAW device performance and robust system packaging, the developed SAW hydrogen sensing system exhibits extremely low baseline noise ($<30 \mu\text{V}$), as demonstrated in Fig. 3b, and the fully integrated SAW hydrogen sensing prototype is shown in Fig. S4c of the supplementary information. The limit of detection (LOD),

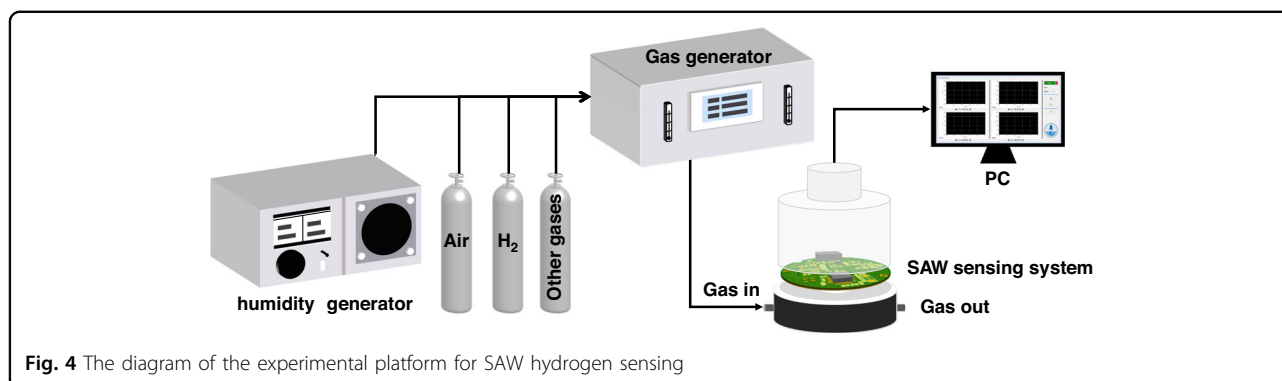


Fig. 4 The diagram of the experimental platform for SAW hydrogen sensing

defined by the International Union of Pure and Applied Chemistry (IUPAC)²⁶ is

$$LOD = \frac{3\sigma}{S_g} \quad (8)$$

Here, σ represents the variance of the system baseline noise, while S_g denotes the sensor sensitivity. A lower baseline noise variance coupled with higher sensor sensitivity contributes to improved detection limits. The baseline noise variance of the sensing system is determined by the stability of both the SAW device and sensing circuitry. As clearly demonstrated in Fig. 3c, which shows the system baseline noise variance at different operating temperatures, there exists an essentially positive correlation between baseline noise variance and operating temperature. Notably, when the device temperature exceeds 120 °C, the baseline noise increases dramatically. This phenomenon can be attributed to two primary factors: first, the elevated temperature of the SAW device may induce heating in the sensing circuitry, thereby amplifying circuit noise²⁷. Second, higher operating temperatures intensify thermal exchange between the SAW device and the ambient environment, leading to phase fluctuations in the SAW device and consequently increasing the system baseline noise. After comprehensive consideration of both sensitivity requirements and the need for low detection limits, the operating temperature of the SAW device in this study set at 120 °C. Moreover, the baseline noise of the sensor demonstrated excellent long-term stability when operating at 120 °C, with a baseline drift of less than 0.6 $\mu\text{V/s}$ (Fig. S5 in the Supplementary Information). Therefore, this temperature represents an optimal balance between achieving sufficient sensitivity while maintaining acceptable noise levels for reliable hydrogen detection.

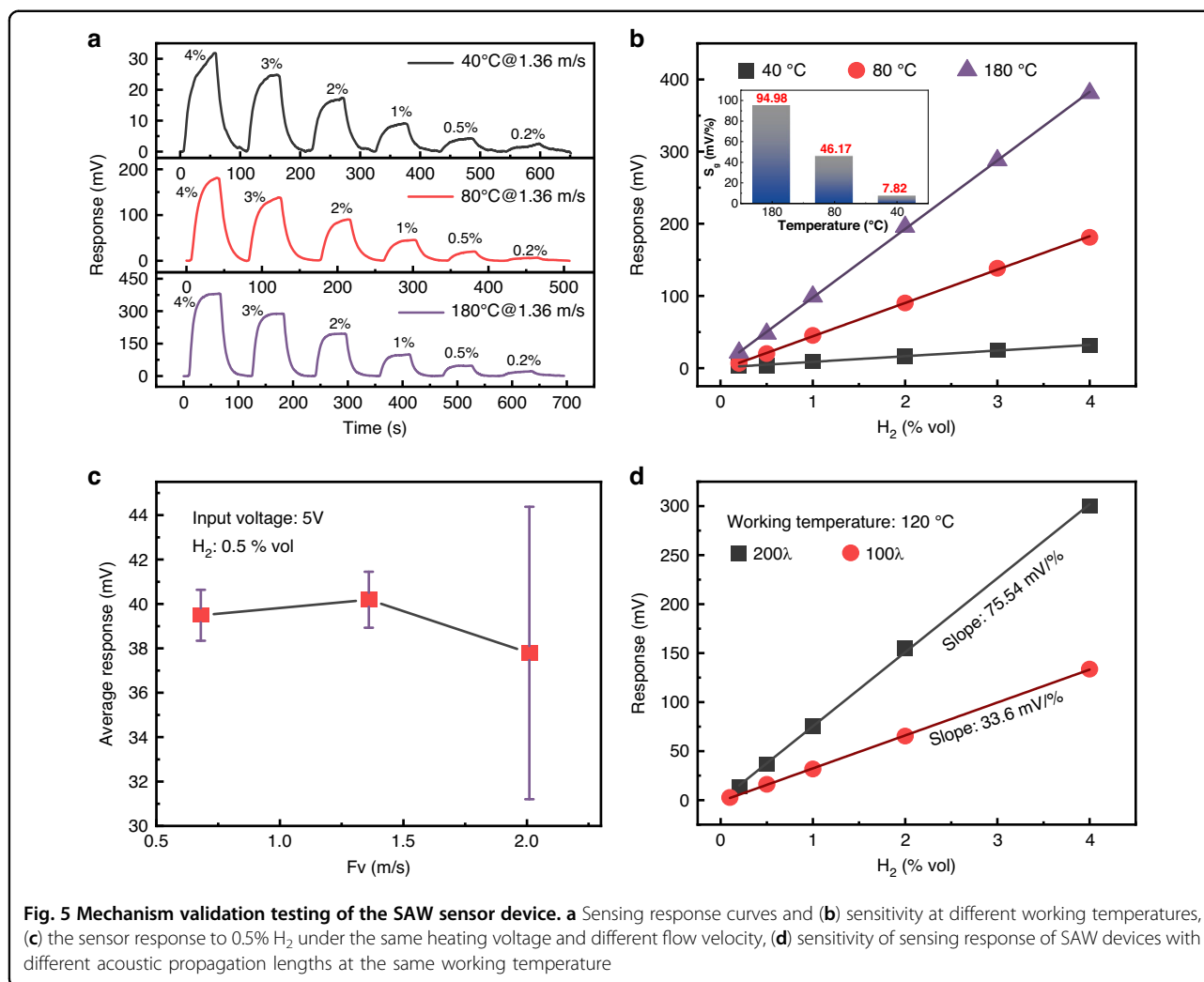
Gas testing platform

To evaluate the hydrogen sensing performance of the designed thermal conductivity-based SAW device, a hydrogen sensing test platform was established as shown

in Fig. 4. All gases used in the experiments, including standard dry air, hydrogen, and four common industrial gases (carbon monoxide (CO), methane (CH₄), carbon dioxide (CO₂), and oxygen (O₂)) for selectivity tests, were supplied by Shanghai Mingyu Industrial Gas Co., Ltd., each with a purity of 99.999%. Standard dry air and hydrogen were precisely mixed using a gas generator (MF-5B, Zhongke Huanyi (Beijing) Metrology Technology Co., Ltd.) equipped with mass flow controllers to automatically produce hydrogen/air mixtures with concentrations ranging from 0 to 100% vol. Additionally, four standard industrial gases were also mixed in-situ with air using the gas generator to produce different gas concentrations for selectivity testing. The humidity generator (EPOCH2017S, Epoch Tech Co., Ltd.) was utilized to produce air with controlled relative humidity levels at room temperature (~25 °C), ranging from 20% to 80% RH, for evaluating the effect of humidity on the SAW hydrogen sensor. The generated gas mixtures were delivered through gas lines to the packaged SAW device. The SAW sensing circuit transmitted the acquired phase information to a host computer via serial communication, enabling real-time SAW phase data acquisition and storage. All gas experiments were conducted within a fume hood to mitigate the risk of hydrogen explosion, while the ambient temperature was maintained at ~25 °C. All experimental equipment was calibrated prior to use.

Mechanism verification

To validate the theoretical model, we first maintained a constant gas flow velocity of 1.36 m/s and measured the response sensitivity of the SAW hydrogen sensor at operating temperatures of 40 °C, 80 °C, and 180 °C (corresponding to different heating voltages). As shown in Fig. 5a, the designed SAW hydrogen sensor exhibited normal and rapid response capabilities within the 0.2–4% vol hydrogen concentration range. The sensitivity values obtained through least-squares fitting (Fig. 5b) clearly demonstrate that higher operating temperatures enhance sensing response sensitivity, consistent with the

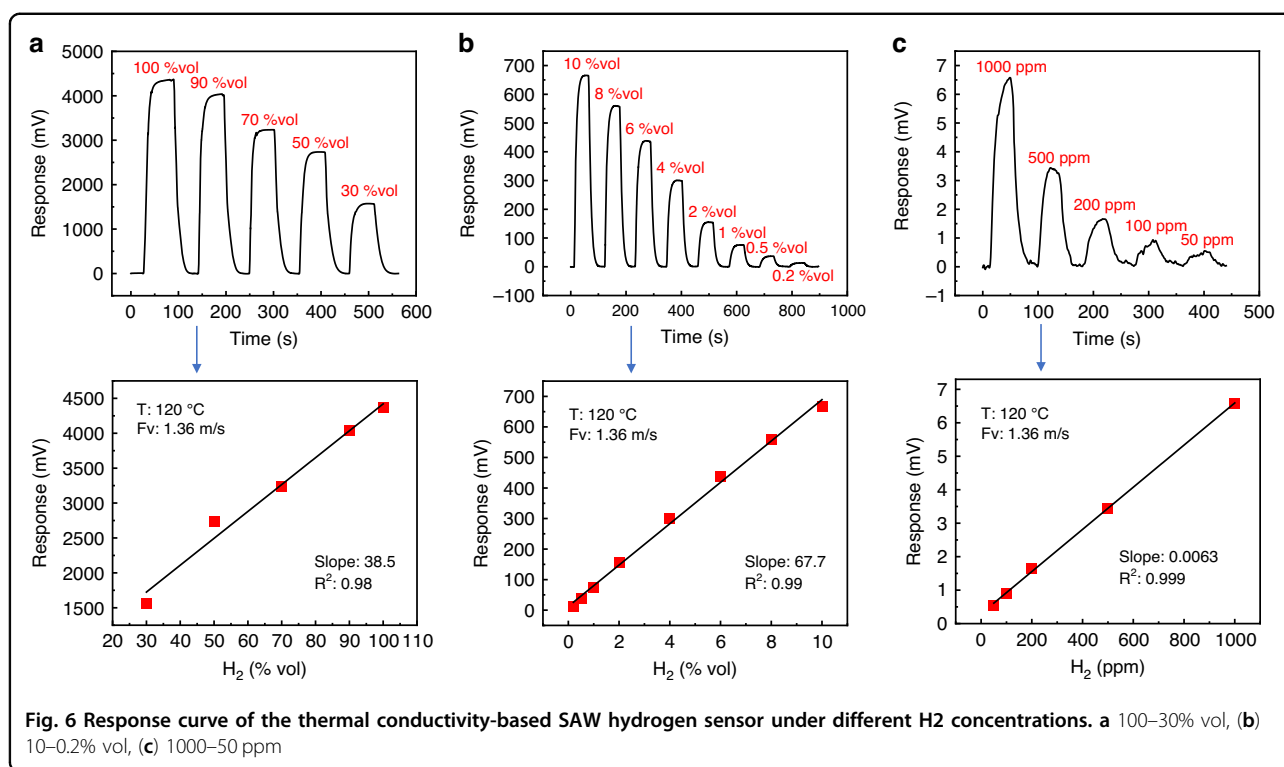


simulation results presented in Fig. 1g. Furthermore, with the SAW device heating voltage held constant, we investigated the effect of flow velocity on sensor response. Figure 5c shows that the SAW sensing sensitivity at different flow velocities initially increases and then decreases with increasing flow rate, matching the simulation results in Fig. 1h. However, experimental observations revealed that higher flow velocities degrade response stability, likely due to intensified temperature fluctuations on the SAW device surface caused by rapid gas flow. This conclusion is supported by the higher baseline noise observed at high flow velocities compared to low flow velocities (Fig. S6 of the supplementary information). To examine the influence of the phase modulation effect on sensitivity, two SAW devices with different propagation lengths were compared. Results in Fig. 5d demonstrate that increasing the acoustic propagation path significantly enhances sensitivity. The device with 200 λ propagation length showed 2.24 times higher sensitivity than the 100 λ device. This improvement stems from enhanced heat exchange

processes and superior phase modulation capability in longer SAW devices. While both devices exhibited similar SAW velocity changes, the extended propagation path provided additional sensitivity gain through phase modulation. After comprehensive evaluation of both sensing sensitivity and operational stability, 200 λ acoustic propagation path, 1.36 m/s flow velocity and 120 °C operating temperature were finally selected as the optimal operating conditions of the SAW sensor, and the power consumption of the sensor is less than 0.4 W.

Detection range and LOD

Based on the optimized structural parameters, the thermal conductivity-based SAW device was exposed to hydrogen concentrations ranging from 100–30% vol, 10–0.2% vol, and 1000–50 ppm to evaluate its detection range. As shown in Fig. 6a–c, the sensor demonstrated rapid and well-shaped responses across the entire tested range (100% vol to 50 ppm), with corresponding sensitivities of 38.5 mV/%, 67.7 mV/%, and 0.0063 mV/ppm, respectively. The



experimental results showed good agreement with theoretical calculations (Fig. S7 of the supplementary information), validating the effectiveness of the theoretical model. Considering the variation in sensitivity across different concentration ranges, the limit of detection (LOD) was calculated to be approximately 6 ppm based on the sensitivity ($S_g=0.0063$ mV/%) obtained from the low-concentration range (Fig. 6c) and the baseline noise variance ($\sigma=13.1$ μ V at ~ 120 °C) shown in Fig. 3c

Response and recovery time

The response time is defined as the duration required to reach 90% of the full-scale signal, while the recovery time refers to the time needed to return to 10% of the baseline value. As shown in Fig. 7a, the designed thermal conductivity-based SAW hydrogen sensor exhibits rapid response (T_{90} : 14.9 s) and recovery (T_{10} : 14.7 s), providing an effective solution for rapid hydrogen detection.

Repeatability

To evaluate sensor repeatability, the device was cyclically exposed to 0.5% vol hydrogen concentration 20 times (Fig. 7b). The SAW sensor demonstrated stable responses (mean: ~ 40 mV) with a repeatability error $<2.4\%$, confirming excellent reproducibility.

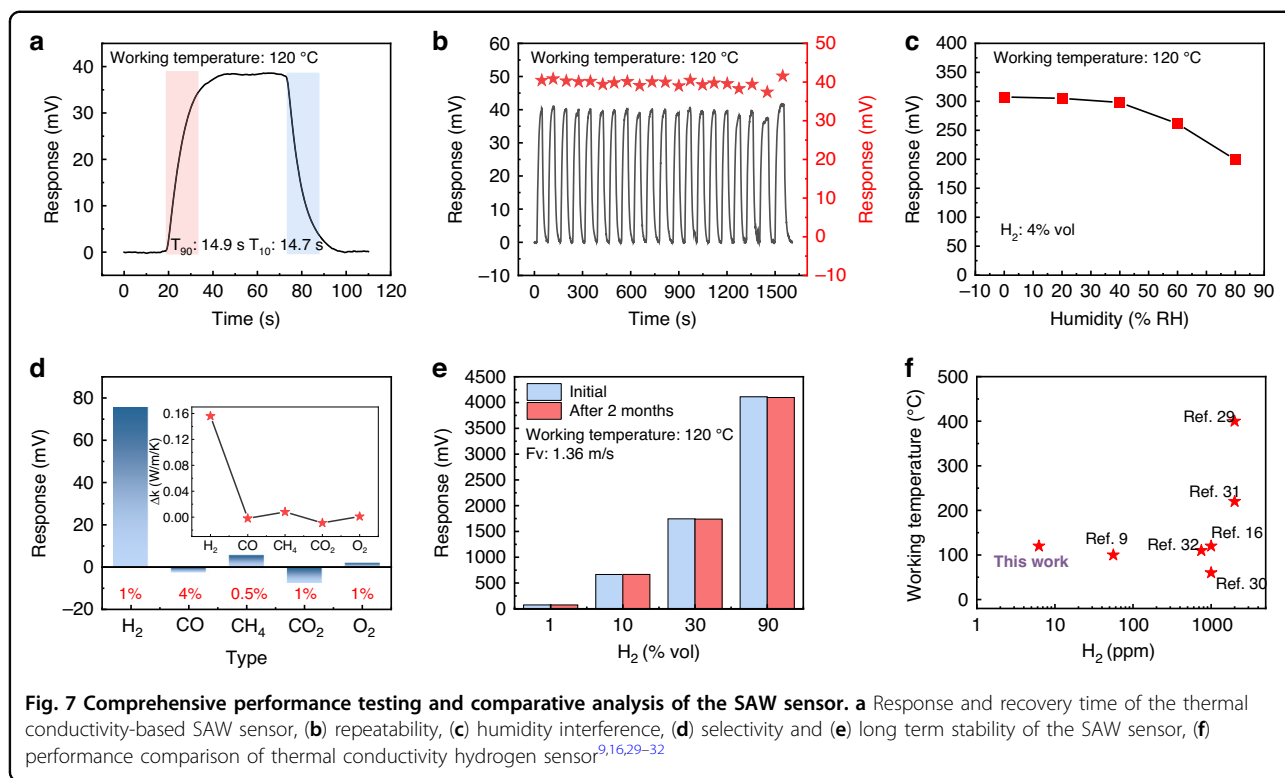
Humidity interference

The prepared SAW hydrogen sensor was exposed to varying relative humidity levels (20–80% RH) to evaluate

humidity interference. As shown in Fig. S8 of the supplementary information, the real-time response curves demonstrate that the sensor maintains excellent response speed and repeatability to 4% vol H₂ across all humidity conditions. However, a gradual decrease in sensing sensitivity was observed with increasing humidity levels (Fig. 7c). From the sensing mechanism perspective, the sensitivity of thermal-conductivity-based SAW hydrogen sensors is positively correlated with changes in gas thermal conductivity. The observed reduction in sensitivity under humid conditions indicates that humidity attenuates the thermal conductivity variation of hydrogen during sensing, which aligns with the humidity-dependent hydrogen thermal conductivity trend²⁸.

Selectivity

Selectivity is critical for gas sensors. Herein, the thermal-conductivity-based SAW hydrogen sensor was systematically exposed to 4% vol CO, 0.5% vol CH₄, 1% vol CO₂, and 1% vol O₂ to evaluate its characteristic responses. The real-time response curves are presented in Fig. S9 of the supplementary information. Figure 7d summarizes the response magnitudes of the sensor to these five gases, demonstrating that the sensor exhibits the highest sensitivity to H₂ gas, which can be attributed to the significant thermal conductivity difference between H₂ and air. Furthermore, the experimental results reveal distinct response magnitudes and directions for the other four gases due to their respective thermal conductivity



differences relative to air (Δk in Fig. 7d). This observation is consistent with the intrinsic operating principle of thermal-conductivity-based gas sensing technology.

Stability

Figure 7e compares the sensor's responses to 1% vol, 10% vol, 30% vol, and 90% vol hydrogen over a two-month interval. Benefiting from the SAW device's low operating temperature ($\sim 120^\circ\text{C}$), superior electrical performance (propagation loss < -10 dB), robust micro-heater, and stable sensing system, the prepared SAW hydrogen sensor exhibits outstanding long-term stability.

Figure 7f benchmarks the sensor against recent thermal conductivity-based hydrogen sensors. The results highlight that the proposed SAW hydrogen sensor featured high sensitivity at a relatively low operating temperature ($\sim 120^\circ\text{C}$). Obviously, the prepared thermal conductivity-based SAW hydrogen sensor achieved wide detection range (up to 100% vol), low detection limit (~ 6 ppm), fast response and recovery time (T_{90}/T_{10} : ~ 15 s), excellent repeatability (repeatability error $< 2.4\%$) and long-term stability. In fact, the sensor designed in this study exhibits excellent sensing performance, primarily due to the precise construction of the thermoacoustic conversion model. This model identifies the key factors and their influencing patterns that affect sensor sensitivity, such as operating temperature, gas flow rate, and acoustic propagation path, which helps to extract optimized design

parameters. The above theoretical model has also been well validated through experiments. Meanwhile, the SAW phase modulation technology proposed in this study has increased the sensitivity of the sensor by more than twice. In addition, the high integration design of the gas chamber-SAW device-signal processing circuit has achieved ultra-low baseline noise ($< 30 \mu\text{V}$), significantly improving the detection limit. In summary, this study has effectively improved the sensitivity and other performance of the thermal conductive SAW hydrogen gas sensor through theoretical model construction and sensor structure design, providing an effective solution for ultra-wide range and high-sensitivity hydrogen leak detection in aerospace, nuclear power, and industrial fields. Future work may focus on researching compensation strategies for environmental temperature and humidity changes from the perspective of surface acoustic wave device architecture or artificial intelligence algorithms, in order to further improve sensing accuracy.

Conclusion

To address the challenge of low sensitivity in existing thermal-conductivity-based surface acoustic wave (SAW) hydrogen sensors, this paper conducts a systematic investigation into high-sensitivity thermal-conductivity-based SAW hydrogen sensors, employing SAW sensing mechanisms, device design and fabrication, and sensing system development as the research framework. By

integrating thermodynamic equations and acoustic wave equation, a comprehensive thermoacoustic response model for thermal conductivity-based SAW hydrogen sensing was completely established. Through comparative analysis of multiple parameters including heating voltage, flow velocity, and device dimensions, the design methodology for high-sensitivity SAW devices under multi-parameter perturbations was clarified and experimentally validate our approach. A phase-detection-based SAW sensing circuit and an integrated SAW hydrogen sensing system were fully developed, demonstrating extremely low baseline noise ($<30 \mu\text{V}$). Experimental results confirm that the fabricated thermal conductivity-based SAW hydrogen sensor achieves ultra-wide detection range (up to 100% vol), low detection limit ~ 6 ppm, and rapid response and recovery time (T_{90}/T_{10} : ~ 15 s) at a relatively low operating temperature (~ 120 °C). Benefiting from low operating temperatures, low acoustic loss and robust SAW sensor and stable SAW sensing system, the sensor simultaneously exhibits outstanding repeatability and long-term stability. This work provides an effective solution for rapid hydrogen leak detection in hydrogen energy safety applications.

Acknowledgements

This work was financially supported by Beijing Natural Science Foundation (No. 1252032, No. QY24359) and the National Natural Science Foundation of China (No. U1837209, 12204510, 12304530, 12404543).

Author contributions

Baile Cui: Writing – review & editing, Writing – original draft, Conceptualization. Wen Wang: Writing – review & editing, Project administration, Funding acquisition, Conceptualization. Lina Cheng: Project administration, Funding acquisition. Xufeng Xue: Software, Resources. Jing Jin: Project administration, Funding acquisition. Yong Liang: Supervision, Methodology. Lintaihui Huang: Project administration, Funding acquisition.

Competing interests

The authors declare no competing interests.

Supplementary information The online version contains supplementary material available at <https://doi.org/10.1038/s41378-026-01199-z>.

Received: 7 August 2025 Revised: 16 December 2025 Accepted: 17 December 2025

Published online: 27 February 2026

References

- Ge, L. et al. A review of hydrogen generation, storage, and applications in power system. *J. Energy Storage* **75**, <https://doi.org/10.1016/j.est.2023.109307> (2024).
- Park, S. W., Kim, J. H. & Seo, J. K. Explosion Characteristics of Hydrogen Gas in Varying Ship Ventilation Tunnel Geometries: An Experimental Study. *J. Marine Sci. Eng.* **10**, <https://doi.org/10.3390/jmse10040532> (2022).
- Park, J., Yoo, Y., Ryu, J. & Lee, H. Study on the Explosion of the Hydrogen Fuel Tank of Fuel Cell Electric Vehicles in Semi-Enclosed Spaces. *Energies* **16**, <https://doi.org/10.3390/en16010241> (2022).
- Liu, K., Jiang, J., He, C. & Lin, S. Numerical analysis of the diffusion and explosion characteristics of hydrogen-air clouds in a plateau hydrogen refuelling station. *International Journal of Hydrogen Energy* **48**, 40101–40116, <https://doi.org/10.1016/j.ijhydene.2023.07.155> (2023).
- Franco, M. A., Conti, P. P., Andre, R. S. & Correa, D. S. A review on chemiresistive ZnO gas sensors. *Sensors Actuators Reports* **4**, <https://doi.org/10.1016/j.snr.2022.100100> (2022).
- Chai, H. et al. Stability of Metal Oxide Semiconductor Gas Sensors: A Review. *IEEE Sensors Journal* **22**, 5470–5481, <https://doi.org/10.1109/jsen.2022.3148264> (2022).
- Wang, B., Sun, L., Schneider-Ramelow, M., Lang, K.-D. & Ngo, H.-D. Recent Advances and Challenges of Nanomaterials-Based Hydrogen Sensors. *Micro-machines* **12**, <https://doi.org/10.3390/mi12111429> (2021).
- Aleazy, E. K. et al. Low-Temperature Hydrogen Sensor: Enhanced Performance Enabled through Photoactive Pd-Decorated TiO₂ Colloidal Crystals. *ACS Sens* **5**, 3902–3914, <https://doi.org/10.1021/acssensors.0c01387> (2020).
- Cho, W., Kim, T. & Shin, H. Thermal conductivity detector (TCD)-type gas sensor based on a batch-fabricated 1D nanoheater for ultra-low power consumption. *Sensors Actuators: Chemical* **371**, <https://doi.org/10.1016/j.snb.2022.132541> (2022).
- Berndt, D. et al. MEMS-based thermal conductivity sensor for hydrogen gas detection in automotive applications. *Sensors Actuators: Physical* **305**, <https://doi.org/10.1016/j.sna.2019.111670> (2020).
- Watanabe, M., Inoue, R., Ichikawa, D. & Furusaki, K. Development of Thermal Conductivity Type Hydrogen Sensor. *ECS Transactions* **28**, 31–42 (2010).
- Cui, B. et al. Review of surface acoustic wave-based hydrogen sensor. *Sensors and Actuators Reports* **7**, <https://doi.org/10.1016/j.snr.2024.100197> (2024).
- Mandal, D. & Banerjee, S. Surface Acoustic Wave (SAW) Sensors: Physics, Materials, and Applications. *Sensors (Basel)* **22**, <https://doi.org/10.3390/s22030820> (2022).
- Yang, Q. et al. Review of surface acoustic wave-based gas sensors. *Sensors International* **7**, <https://doi.org/10.1016/j.sintl.2025.100348> (2026).
- Devkota, J., Mao, E., Greve, D. W., Ohodnicki, P. R. & Baltrus, J. A surface acoustic wave hydrogen sensor with tin doped indium oxide layers for intermediate temperatures. *Sensors Actuators: Chem.* **354**, <https://doi.org/10.1016/j.snb.2021.131229> (2022).
- Anisimkin, V. I., Penza, M., Osipenko, V. A. & Vasanelli, L. Gas Thermal Conductivity Sensor Based on SAW. *IEEE TRANSACTIONS ON ULTRASONICS, FERROELECTRICS, AND FREQUENCY CONTROL* **42**, 978–980 (1995).
- Tooru Nomura, A. S., Koichi Koyama. in *IEEE International Frequency Control Symposium* (2007).
- Durani, F., Mainuddin, Mittal, U., Kumar, J. & Nimal, A. T. Use of Surface Acoustic Wave (SAW) for Thermal Conductivity Sensing of Gases – a Review. *IETE Technical Review* **38**, 611–621, <https://doi.org/10.1080/02564602.2020.1819888> (2020).
- Oliva, A. I. & Lugo, J. M. Measurement of the Temperature Coefficient of Resistance in Metallic Films with Nano-thickness. *Int. J. Thermophysics* **37**, <https://doi.org/10.1007/s10765-016-2046-0> (2016).
- ROBERT F MILSOM, N. H. C. R., AND MARTIN REDWOOD Analysis of Generation and Detection of Surface and Bulk Acoustic Waves by Interdigital Transducers. *IEEE TRANSACTIONS ON SONICS AND ULTRASONICS* **24**, 147–166 (1977).
- Smith, R. T. & Welsh, F. S. Temperature Dependence of the Elastic, Piezoelectric, and Dielectric Constants of Lithium Tantalate and Lithium Niobate. *Journal of Applied Physics* **42**, 2219–2230, <https://doi.org/10.1063/1.1660528> (1971).
- Watada, K. et al. Power transmission characteristics of EWC-SPUDT SAW filters fabricated for multiplex transmission system of inverter gate drive circuits. *Japanese J. Applied Phys.* **59**, <https://doi.org/10.35848/1347-4065/ab85ab> (2020).
- Sun, X. et al. Analysis and Design of Single-Phase Unidirectional Transducers with High Directivity. *Applied Sci.* **11**, <https://doi.org/10.3390/app11167500> (2021).
- Wen, W., Shitang, H., Shunzhou, L., Minghua, L. & Yong, P. Enhanced sensitivity of SAW gas sensor coated molecularly imprinted polymer incorporating high frequency stability oscillator. *Sensors and Actuators B: Chemical* **125**, 422–427, <https://doi.org/10.1016/j.snb.2007.02.037> (2007).
- Cui, B. et al. Conductive metal-organic framework for ppb-concentration and highly selective SAW hydrogen sulfide sensing at room temperature. *Sensors Actuators: Chemical* **423**, <https://doi.org/10.1016/j.snb.2024.136817> (2025).
- Currie, L. A. Nomenclature in evaluation of analytical methods including detection and quantification capabilities (IUPAC Recommendations 1995). *Analytica Chimica Acta* **391**, 105–126 (1999).

27. Ren, Z. et al. Temperature and Humidity Effects on SAW Hydrogen Sensor and Compensation Method. *IEEE Sensors Journal* **24**, 22317–22325, <https://doi.org/10.1109/jsen.2024.3408283> (2024).
28. Emperhoff, S., Eberl, M., Dwertmann, T. & Wollenstein, J. On the Influence of Humidity on a Thermal Conductivity Sensor for the Detection of Hydrogen. *Sensors (Basel)* **24**, <https://doi.org/10.3390/s24092697> (2024).
29. Xie, D. et al. in *2024 IEEE 37th International Conference on Micro Electro Mechanical Systems (MEMS)* 879–882 (2024).
30. Occelli, C., Fiorido, T., Perrin-Pellegrino, C. & Seguin, J.-L. Sensors for anaerobic hydrogen measurement: A comparative study between a resistive PdAu based sensor and a commercial thermal conductivity sensor. *Int. J. Hydrogen Energy* **48**, 17729–17741, <https://doi.org/10.1016/j.ijhydene.2023.01.193> (2023).
31. Zhang, Y. et al. High Heat Transfer Efficiency MEMS Thermal Conductivity Gas Sensor for Hydrogen. *IEEE Sensors Journal* **24**, 29678–29686, <https://doi.org/10.1109/jsen.2024.3443456> (2024).
32. Wu, Z. et al. Ultra-Low-Power, Extremely Stable, Highly Linear-Response Thermal Conductivity Sensor Based on a Suspended Device with Single Bare Pt Nanowire. *ACS Sens* **9**, 4721–4730, <https://doi.org/10.1021/acssensors.4c01111> (2024).